Incorporation of Na and S in bamboo coral skeletons

Sebastian Flöter [a,b,c,*], Jan Fietzke [a], Marcus Gutjahr [a], Gernot Nehrke [d], Anton Eisenhauer [a]

[a] *GEOMAR Helmholtz Centre for Ocean Research Kiel, Wischhofstr. 1-3, 24148 Kiel, Germany*
[b] *Department of Earth Sciences, Vrije Universiteit Amsterdam, De Boelelaan 1085, 1081 HV Amsterdam, The Netherlands*
[c] *Department of Earth Sciences, University of Geneva, Rue des Maraîchers 13, 1205 Geneva, Switzerland*
[d] *Alfred Wegener Institute Helmholtz Centre for Polar and Marine Research, Am Handelshafen 12, 27570 Bremerhaven, Germany*

ARTICLE INFO

ABSTRACT

Ocean environmental conditions can be inferred from the chemical composition of bamboo coral skeletons. The high magnesium calcite internodes of these long-living octocorals may therefore represent a potential archive for seawater properties such as salinity or temperature where instrumental time series are absent. To extend these time series into the past using a natural archive the principles of temperature and salinity signal incorporation into cold-water coral skeletal material need to be investigated. Since skeletal Na and S concentrations have been proposed as environmental proxies, we mapped the spatial distribution and concentration of these elements in two Atlantic specimens of *Keratoisis grayi* (family Isididae). These measurements were conducted with an electron microprobe applying a spatial resolution of 4 μm. The mean apparent distribution coefficient of Na/Ca for the two samples was within 2.5 and $2.8*10^{-4}$, while that of S shows a similar depletion relative to seawater with 3.8 and $3.6*10^{-3}$. The two elements show an inverse correlation in bamboo coral skeletons. The mean apparent distribution coefficient of Na is similar to that of abiotic calcites. This similarity can be interpreted as the absence of significant vital effects for skeletal Na/Ca. Hence it corroborates the idea that the average skeletal composition of bamboo corals holds the potential to record past seawater conditions. In contrast, it appears unlikely that the spatial variations of the element distribution of seemingly simultaneously precipitated material along growth rings are exclusively controlled by environmental factors. We further exclude Rayleigh fractionation, ion-specific pumping, and Ca/proton exchange as the driver of Na and S distribution in bamboo corals. Instead, we adapt a calcification model originally proposed for scleractinians to bamboo corals. This model can explain the observed distribution of Na and S in the skeleton by a combination of Ca/proton pumping, bicarbonate active transport, and the formation of an organic skeletal matrix. The adapted model can further be used to predict the theoretical behaviour of other elements and disentangle vital effects from external factors influencing compositional features. It is therefore a useful tool for future studies on the potential of bamboo corals as environmental archives.

1. Introduction

The elemental composition of deep-sea coral skeletons may hold vital information about deep-water environmental conditions. These include e.g. temperature or nutrient availability on timescales of decades to centennials and depth where instrumental records are missing (Robinson et al., 2014). It is key to assess if and how sensitive a reconstructed geochemical signature responds to external environmental conditions, whether it is merely controlled by internal physiological processes or a combination of both internal and external controls. For this purpose, the calcification process of the skeleton and its influence on the elemental composition, the so-called vital effect (Urey et al., 1951),

needs to be fully understood. The advantage of using bamboo corals as environmental proxy recorders is their long life span of up to 300 years (Andrews et al., 2009; Hill et al., 2011), they are sessile on hardgrounds and the wide habitat depth range of less than 10 to over 3000 m (Bostock et al., 2015; Thresher et al., 2016). Closer investigation of the geochemical controls over cold-water coral growth is not only important for further developing deep-water corals as environmental proxy archives. Knowledge of their calcification mechanism concerning environmental demands is also important to evaluate their susceptibility to ocean acidification, warming, or deoxygenation (Roberts et al., 2016).

The potential of the calcitic skeleton of bamboo coral as a proxy archive has been investigated using for example Ba, Mg (Flöter et al.,

---

2019; Thresher et al., 2016), and Sr concentrations (Hill et al., 2012) as well as B isotopes (Farmer et al., 2015a). The internodal concentration of Na was investigated by Rollion-Bard et al. (2017). Nevertheless, it is still unknown how Na and S are distributed in the calcitic skeleton of bamboo corals. Sodium as the most abundant cation in the ocean has a concentration of 0.486 mol kg^{-1} at a salinity of 35 (Millero et al., 2008) and a mean residence time of 44*10^6 years (Lécuyer, 2016), while S in the form of sulfate is the second most abundant anion with a concentration of 0.03 mol kg^{-1} (Millero et al., 2008) and a mean residence time of 9*10^6 years (Lécuyer, 2016). The incorporation of Na and S into biogenic and abiogenic calcite was found to be dependent on several factors. Studies on biogenic calcite reported a relationship of skeletal Na/Ca to seawater salinity for several recent calcifying species. The clearest indication into this direction comes from recent studies on foraminifera. A positive salinity-Na/Ca correlation was observed e.g., by Wit et al. (2013), Allen et al. (2016), and Mezger et al. (2016). Apart from foraminifera, other species were also found to show a positive Na/Ca correlation with salinity. Gordon et al. (1970) presented similar findings from barnacle shells, while brachiopods may also hold potential for recording seawater salinity (Rollion-Bard et al., 2019).

Skeletal Na concentrations were also explained by a variety of other factors than salinity. According to Hauzer et al. (2018), the Na/Ca ratio in tests of the foraminifera *Operculina ammonoides* is positively correlated with the Na/Ca ratio of seawater which does not vary with salinity. Iglikowska et al. (2018) found an inverse correlation between Na/Ca ratios and barnacle size. Also, acidification was found to raise the shell Na/Ca ratio of the bivalve *Mytilus edulis* by Zhao et al. (2017), while Ballesta-Artero et al. (2018) suggested that the Na/Ca ratio is influenced by the growth rate for the same species.

Abiotic precipitation experiments on the incorporation of Na into calcite were conducted by (Kitano et al., 1975) and (Okumura and Kitano, 1986), who found the Na/Ca ratio to be influenced by the Na content of the parent solution. Similar to these studies, Ishikawa and Ichikuni (1984) found the Na/Ca ratio of the precipitate to rise with increased Na content in the parent solution. Conversely, the Na/Ca ratio reaches saturation in the calcite phase at about 0.2 mol L^{-1} aqueous Na, hence below seawater concentrations. The crystal growth rate was found to be the driver of Na incorporation in the experimental setup of Busenberg and Plummer (1985) resulting in a positive correlation.

Although representing different mineralogy, studies on Na/Ca in biogenic aragonite (e.g. Mitsuguchi et al., 2010; Mitsuguchi and Kawakami, 2012; Rollion-Bard and Blamart, 2015) found incorporation by lattice defects or ion adsorption, and kinetic effects as possible explanations for increased Na incorporation.

The incorporation of S into biogenic calcite is less well understood to date. The amount of S incorporated in biogenic calcite appears to be influenced by the carbonate chemistry of the calcifying solution (van Dijk et al., 2017, 2019) and organic matrix association (e.g., Dauphin, 2006; Vielzeuf et al., 2013; Nguyen et al., 2014). Although S can be associated with organic compounds in biogenic calcite, it has equally been suggested to be present in inorganic form as so-called structurally substituted S (e.g., Pingitore et al., 1995; Cusack et al., 2008; Fichtner et al., 2018). In the skeletons of calcitic octocorals both organic and inorganic bound S is present (e.g., Vielzeuf et al., 2013; Nguyen et al., 2014; Balan et al., 2017). From an evolutionary point of view, it also becomes evident that the organic matrix is an important constituent of the calcitic skeleton. Le Roy et al. (2021) report that the calcitic skeleton of *Corallium rubrum* — a calcitic octocoral species — results from secondary calcification of an ancestral horny axis.

Precipitation experiments on abiotic calcite formation found that the composition of the precipitation solution impacts the composition of the formed calcite. It was observed that less S is incorporated with rising Na in precipitation solution (Kitano et al., 1975). Further, it has been reported that the S content in calcite increases with higher solution sulfate concentration until a molar ratio of S to Ca level of 4 to 5% was reached (Okumura et al., 2018). Calcite crystal growth rate was found to be one

driver of sulfate incorporation in the precipitation experiments of Busenberg and Plummer (1985). Conversely, Wynn et al. (2018) reported that pH is the main driver of sulfate incorporation followed by increased incorporation with rising precipitation rates due to defect site incorporation.

A meaningful reconstruction of carbonate archives and the understanding of its calcification go hand in hand. Therefore, the environmental driver and the biological processes performing and maintaining the calcification of an organism must be understood. Although models for scleractinians have previously been developed, currently no calcification model exists for calcitic octocorals.

In this study, we investigate the Na/Ca and S/Ca spatial distribution in the skeleton of two bamboo corals of the genus *Keratoisis* with a focus on their environmental proxy potential. Further, we test the ability of the recent coral calcification models of McCulloch et al. (2017) and Giri et al. (2019) to correctly predict the Na/Ca and S/Ca distribution in the skeleton. For this purpose, we used high-resolution element mapping techniques (laser ablation inductively coupled mass spectrometry (LA-ICPMS) and electron microprobe (EMP)) combined with confocal Raman microscopy (CRM) to gain insight into potential processes that control the incorporation of Na and S into the skeleton.

2. Oceanographic setting, material, and methods

2.1. Specimen and sample

We used two specimens of *Keratoisis grayi* (family Isididae) collected in the North Atlantic (Fig. 1). Sample YPM 37031 was dredged 2006 on Bear Seamount (40.257°N, 67.691°W) from about 950 m depth during R/V Delaware cruise DE 04–08. After collection, it was frozen, treated with 70% alcohol, and stored dried. The second sample (USNM 10496) was collected in 1885 on the Blake Plateau (30.733°N, 79.433°W) in approximately 805 m water depth. This sample was collected during a cruise of the United States Fish Commission and stored in ethanol. For both samples, the mean growth rate was previously determined using radiocarbon (Farmer et al., 2015b). Both samples were covered with coral tissue at collection and thus are assumed to have been alive at the time of collection. No signs of bioerosion or diagenetic alteration can be found in the samples.
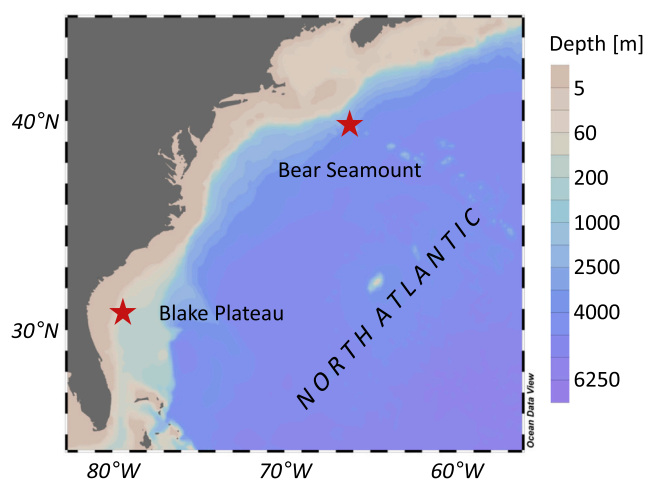

Fig. 1. Sampling sites (red stars) of the two investigated bamboo corals from the Blake Plateau and the Bear Seamount. (For interpretation of the references to colour in this figure legend, the reader is referred to the web version of this article.)

2.2. Oceanographic setting (Blake Plateau and Bear Seamount)

The Blake Plateau in the South Atlantic Bight is overflown by the Florida Current and represents a highly variable environment. The bottom water temperature at the sampling site shows a total variation of 3.9 °C around an annual mean of about 7.9 °C at the nearest long-time mooring station (Lee and Waddell, 1983), while frequent CTD casts carried out between 2001 and 2017 show a total variation of 2.0 °C at 725 m ($n = 64$). The salinity variation in the Florida Straits given as 2SD was measured to be about 0.05 with a total range of 0.21 PSU around an annual mean of 34.93 PSU (data were collected as part of NOAA's Deep Western Boundary Current Time Series (DWBC) and are available at www.aoml.noaa.gov/phod/wbts/data). The collection date of the historic sample predates available instrumental data. Nevertheless, a potential T and S change since the collection is assumed to be negligible for our investigation on the spatial element distribution and the calcification process.

Bear Seamount is part of the New England Seamount Chain and is located 50 km off the shelf break of Georges Bank. It is occupied by the Gulf Stream and exhibits a more stable environment in comparison to the Blake Plateau. Temperature data were taken at 1000 m depth at mooring station W1 (39.601°N, 69.717°W) from 2008 to 2013 and is a part of the long-time observing system Line W south of New England carried out by Woods Hole Oceanographic Institution (www.whoi.edu/science/PO/linew/index.htm). The total recorded temperature variation at this location is 0.9 °C and with a mean of 4.3 ± 0.2 °C (2SD) and the salinity variation is 0.02 (2SD) (total range of 0.13) around a mean of 34.96 PSU. The mean temperature is, therefore, higher on the Blake Plateau than on Bear Seamount with a smaller variation at the latter location. The same trend in variation is observed for salinity at the sampling sites but with only marginally different mean salinities.

2.3. Electron microprobe mapping (Na, S, Ca)

The samples were horizontally cut from the basal internode of each specimen, embedded in Araldite 2020 resin (Huntsman International LLC). The embedded sections were ground down and then polished in a graded series with Struers Dia Pro polishing emulsions (9, 3, and 1 μm) with a Struers TegraPol polishing machine. The embedded sample was rinsed after each polishing step with demineralised water and dried with pressurised air. After final polishing, the sample was stored until measurement in a bolted vial.

Sodium, S, and Ca were mapped by EMP using a JEOL JXA 8200. Before analysis, the sample was sputter-coated with carbon to avoid sample charging. Desired elements were measured simultaneously by wavelength-dispersive spectrometers. Na was measured using TAPH (thallium acid phthalate, high intensity) and TAP (thallium acid phthalate), Ca using PETJ (pentaerythritol), and S using two times PETH (pentaerythritol, high intensity) as diffraction crystals, respectively. A high-resolution transect across the sample radius was performed with an electron beam diameter of 4 μm, a dwell time of 50 ms, and a current of 50 nA at 15 kV accelerator voltage. All the investigated areas were scanned five times. This, together with multiple simultaneous measurements of Na and S, was done to increase the count rates and with that to minimise the statistical uncertainty to receive a spatially better-resolved map. The dwell time and current were chosen to assure high signal intensity without damaging the carbon coating or significant loss of Na during mapping. Concentrations were calculated by mapping different carbonate and silicate reference materials under the same conditions as the samples (see Appendix A, Fig. A.6, A.7, and A.8). The mapped area for the Blake Plateau sample is 2.00×4.44 mm, while on the Bear Seamount sample an area of 2.00×6.50 mm was mapped.

Based on counting statistics, the two-sided 2 σ relative variation of a single pixel's Na/Ca is $\approx 23\%$ and $\approx 19\%$ for S/Ca. These values improved about 2.7-fold using a 3×3 Gauß smoothing (weighting: 1, 2, 4) for the elemental maps resulting in a 2 σ relative variation of $\approx 9\%$ for Na/Ca and $\approx 7\%$ for S/Ca.

2.4. LA-ICP-MS (Na and Ca mapping)

Besides following the EMP element mapping approach, the distribution of ^{23}Na and ^{44}Ca was also mapped on the polished and carbon-coated sample of the Bear Seamount sample by LA-ICP-MS. The additional mapping by laser ablation was carried out to exclude potential surface contamination. Ablation was carried out using a Nu AttoM sector field ICP-MS coupled to an Electro Scientific Industries NWR 193 nm excimer laser. Plasma conditions were tuned for hot plasma conditions according to Fietzke and Frische (2016). The data were acquired with a scan speed of 25 μm s^{-1}, a laser pulse rate of 20 Hz, a fluence of about 3 J cm^{-1}, and a laser beam diameter of 32 μm. Each laser line was shifted by 30 μm so that it overlapped with the neighbouring line by two μm. Before the acquisition of the two maps, a pre-ablation was carried out on the same sample area. Pre-ablation was performed with a scan speed of 200 μm s^{-1}, a laser pulse rate of 15 Hz, a fluence of 3 J cm^{-1}, and a beam diameter of 44 μm. The sample transects comprised three neighbouring maps recorded subsequently. Before and after each of these three maps a NIST SRM 610 glass standard was measured under the same ablation conditions (Table A.1).

The data reduction was performed as outlined in Flöter et al. (2019). ^{44}Ca was used as an internal standard and NIST SRM 610 was employed for external calibration. The precision of the element concentration based on the reproducibility of the NIST SRM 610 standard was calculated to be 9.5% (RSD, $n = 12$). The three separate sections of each map were stitched together after background correction of the raw counts. Subsequently, both maps of the Bear Seamount sample were added to each other, and drift corrected. After drift correction, the maps were smoothed with three times three cells Gaussian filter, and finally, the molar concentration was calculated.

2.5. Confocal Raman microscopy

To determine the distribution of organic material and crystal orientation (as described in Nehrke and Nouet (2011)) the polished sample was imaged employing confocal Raman microscopy. The measurements were performed using a WITec alpha 300 R instrument equipped with a diode laser having an excitation wavelength of 488 nm. The spectrometer had a grating of 600 mm^{-1} blazed at 500 nm. We used enhanced fluorescence in the spectral range of 2000 to 2400 cm^{-1} to map the distribution of organic matter. This was done following Wall and Nehrke (2012) who found that enhanced fluorescence correlated with organic matter content in the skeleton of corals. Overview images were recorded with an integration time of 0.2 s every 10 μm using a Zeiss 20× Epiplan lens (NA 0.4). For the higher resolved maps, an integration time of 0.2 s every 1.2 μm was used with a Zeiss 60× Lens Epiplan-NEOFLUAR Pol lens (NA 0.8).

3. Results

3.1. Spatial distribution and concentration of Na (EMP and LA-ICPMS)

The concentrations of Na in the Bear Seamount sample were calculated based on LA-ICPMS and EMP measurements. For that, we assumed that the sample consists only of calcium carbonate and one mole Ca corresponds to one mole of skeletal material. EMP maps show a mean Na concentration of 12.9 ± 3.3 mmol mol^{-1} (2SD), which matches concentrations determined via LA-ICPMS of 14.4 ± 2.9 mmol mol^{-1} (2SD) from two overlaying maps. In comparison to LA-ICPMS, the EMP results show a finer resolved but similar spatial Na distribution. Both methods integrated over approximately the same depth range of 2 μm. The LA-ICPMS penetration depth was approximated based on average ablation yields according to Eggins et al. (1998) and for EMP based on Kanaya and Okayama (1972). Based on the acquisition of Na/Ca with LA-ICPMS

and EMP we can exclude any surface contamination. This exclusion can be done since LA-ICPMS revealed the same mean Na/Ca ratios for both mappings and a similar spatial distribution of Na as the EMP measurements (see Appendix A, Fig. A.9).

The sample from the Blake Plateau, on which exclusively microprobe measurements were conducted, shows a mean Na concentration of 11.5 ± 3.9 mmol mol^{-1} (2SD). The apparent distribution coefficient of biogenic carbonates is commonly calculated similarly to abiogenic carbonates via relating the skeletal Na to Ca ratio to that of the surrounding seawater. The calculation of the mean apparent distribution coefficient K_D^* was done using Eq. 1 where E is the molar concentration of a given trace element of interest in the skeleton (SK) and seawater (SW), respectively. Based on the microprobe measurements we found a mean K_D^* of 2.5×10^{-4} ranging from 1.9 to 3.2×10^{-4} and 2.8×10^{-4} ranging from 2.2 to 3.3×10^{-4} for the Blake Plateau and Bear Seamount sample, respectively. The ranges are calculated based on the 5 and 95% quantile of the smoothed molar Na/Ca ratios. For the calculation, we used a molar Na to Ca ratio in seawater of 45.6 mol mol^{-1} with concentrations from Millero et al. (2008).

$$K_D^* = \frac{\left(\frac{E}{Ca}\right)_{SK}}{\left(\frac{E}{Ca}\right)_{SW}} \tag{1}$$

Within the Bear Seamount sample (Fig. 2b) a high Na concentration ($\approx$ 20 mmol mol^{-1}) ring at about 5 mm from the rim can be observed while the lowest values ($\approx$ 7 mmol mol^{-1}) were found in the outer 1.5 mm of the section. The zig-zag pattern recorded from 5.2 to 1.3 mm from the rim can only be seen in the high-resolution map from EMP measurements. Growth rings and ring-parallel patterns can also be observed on the Blake Plateau sample (Fig. 2a). The highest values were measured around the central channel with $\approx$ 22 mmol mol^{-1} while the lowest of $\approx$ 5 mmol mol^{-1} is found in ring structures from 2.1 mm from the rim to the rim itself.

The distribution of Na/Ca is mainly driven by the variation of Na in the sample (see Fig. A.10 in Appendix A). The relative variation of Ca (EMP) calculated from the 5 and 95% percentile is much smaller than the corresponding variation in Na. The relative Ca variation accounts for only 2.4% on the Bear Seamount sample and 2.6% on the Blake Plateau. In turn, the Na content in these specimens varies with 41% and 45%, respectively. The absolute variation for Na is 4.9 mmol mol^{-1} on the Bear Seamount sample and 4.5 mmol mol^{-1} on the Blake Plateau sample and therefore smaller than that of Ca (22.1 and 23.4 mmol mol^{-1},

respectively). This can be explained with the incorporation of other elements such as Mg or Sr. Sodium and Ca are significantly ($p < 0.001$, t-test) inversely correlated suggesting a linear relationship with an R^2 of 0.46 and 0.47 on the Blake Plateau sample and the Bear Seamount sample, respectively (see Fig. A.11 in Appendix A). This correlation leads to a slight deviation from the 1:1 Na - Na/Ca line but has only a marginal impact on the chemical patterns (Fig. A.10).

3.2. Spatial distribution of fluorescence and S

The concentration of S measured by EMP revealed a mean of 9.8 ± 1.9 mmol mol^{-1} (2SD) for the Bear Seamount coral and 10.3 ± 2.1 mmol mol^{-1} (2SD) for the Blake Plateau sample (Fig. 2c and d). The highest concentrations on the Bear Seamount sample of about 12 mmol mol^{-1} are mostly found in a broad band in the outer 0.9 mm from the rim and a less broad band about 1.7 mm from the rim. An additional single thin band of increased S concentrations can also be found about 1.3 mm from the centre. Lower concentrations down to about 7 mmol mol^{-1} can be observed between these features on the sample from the Bear Seamount. The Blake Plateau sample shows the lowest values in a region of about 0.2 mm around the central channel containing $\approx$ 7 mmol mol^{-1}. The highest concentrations were observed within thin bands in the outer 2.6 cm with up to $\approx$ 13 mmol mol^{-1}.

The mean K_D^* was calculated to be 3.8×10^{-3} ranging from 3.2 to 4.5×10^{-3} for the Blake Plateau sample and 3.6×10^{-3} ranging from 3.2 to 4.2×10^{-3} for the Bear Seamount sample based on an S to Ca ratio of 2.75 mol mol^{-1} in seawater according to Millero et al. (2008). The ranges are calculated based on the 5 and 95% quantiles of the smoothed molar S/Ca ratios.

Like for Na, the S/Ca ratio is mainly driven by the variation of S in the sample. The total S variation on the sample based on the 5 and 95% quantile is 18% in the Bear Seamount and 21% in the Blake Plateau sample. Therefore, it is higher than the accompanied relative Ca concentration variation of 2.4 and 2.6% respectively.

The elemental distribution patterns of Na and S are mirrored by confocal Raman microscopy fluorescence maps (Fig. 3). Fluorescence and S generally show a positive correlation, while the fluorescence maps provide a better-resolved picture of the distribution. For example, banded structures originating from desmocyte attachment of about 15 ± 9 µm (2SD, n = 38) length can be resolved (Fig. 3c). These bands eventually form the superordinate ring and zig-zag structures at the millimetre scale (Fig. 3b). Broad low-S zig-zags mostly in the right half of Fig. 3a are surrounded by thin borders of higher S concentrations. This is mirrored in the CRM mappings with a higher fluorescence.
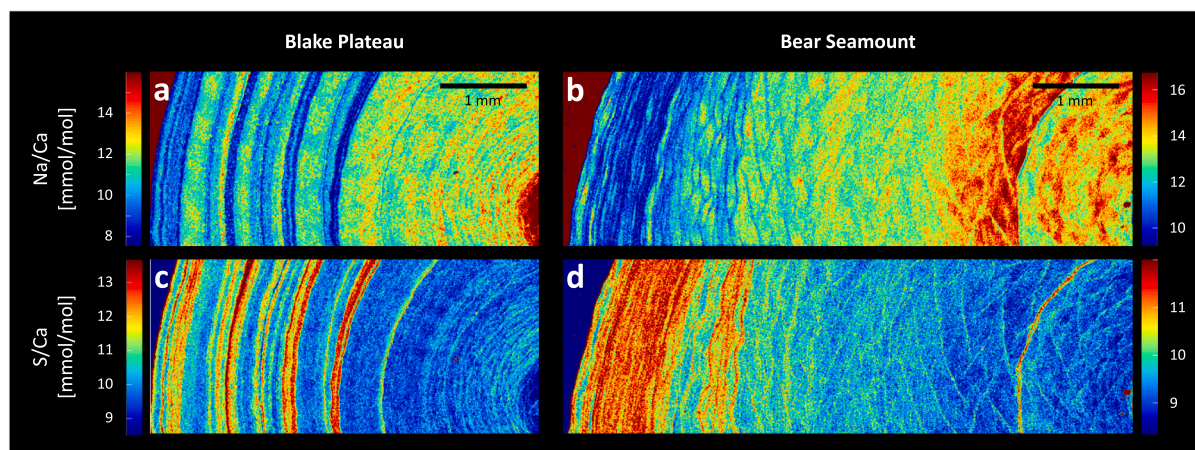
Fig. 2. EMP maps of Na/Ca and S/Ca on the bamboo coral samples from the Blake Plateau (a and c) and Bear Seamount (b and d). The maps show the composition of a transect from the rim (left) to the centre (right). The growth direction of both sample sections is to the left of the figure. (For interpretation of the references to colour in this figure legend, the reader is referred to the web version of this article.)
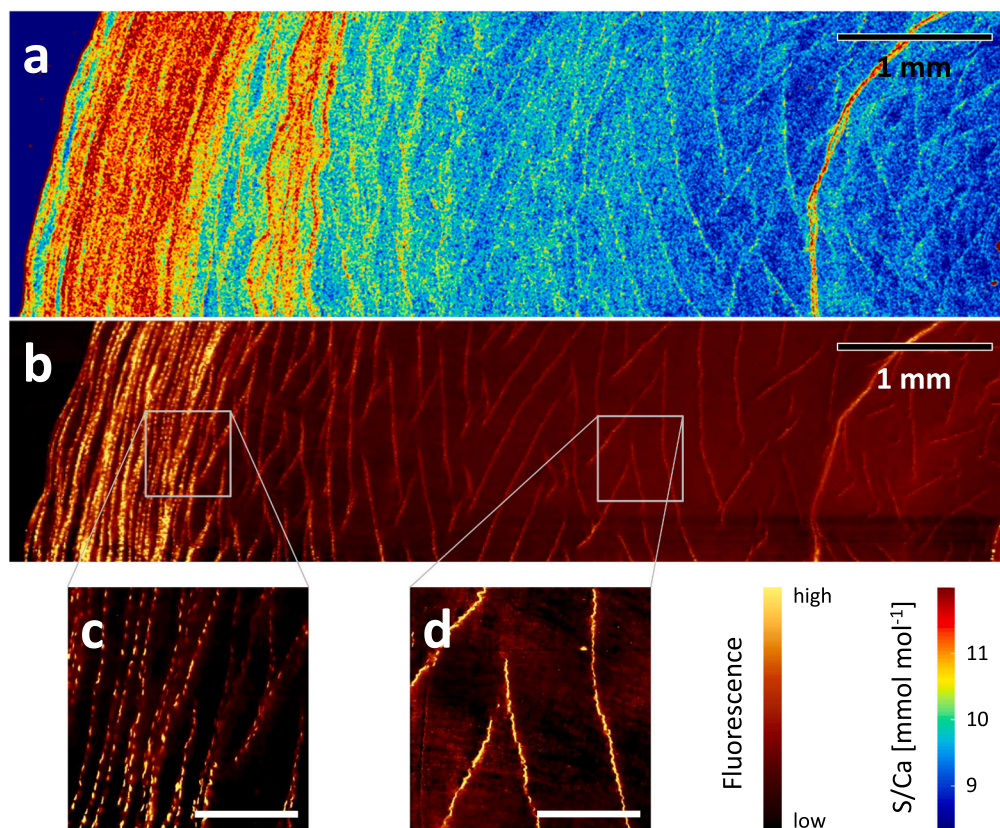
Fig. 3. S/Ca and fluorescence of approximately the same area on the bamboo coral sample from Bear Seamount. The comparison shows the similarity in distribution indicating a spatial relationship of S and organic matter (a and b). Insets (c) and (d) provide a cl closer look into the small-scale structure of the high-fluorescence bands. The bars in (c) and (d) denote the length of 250 μm. (For interpretation of the reference to colour, the reader is referred to the web version of this article.)

3.3. Na to S ratio

The mean ratio of Na to S in the Blake Plateau sample is 1.13 ± 0.47 and in the Bear Seamount sample 1.34 ± 0.50 mol mol^{-1} (2SD). As evident from Fig. 2, S is inversely correlated with Na with a slight sigmoidal distribution (Fig. 4). The frequency distribution was created

with an integration interval of 0.1 mmol mol^{-1} for S/Ca and Na/Ca and a minimum of ten displayed counts for each interval.

3.4. Crystallite shape and orientation

The intensity of a Raman peak depends on the orientation of the
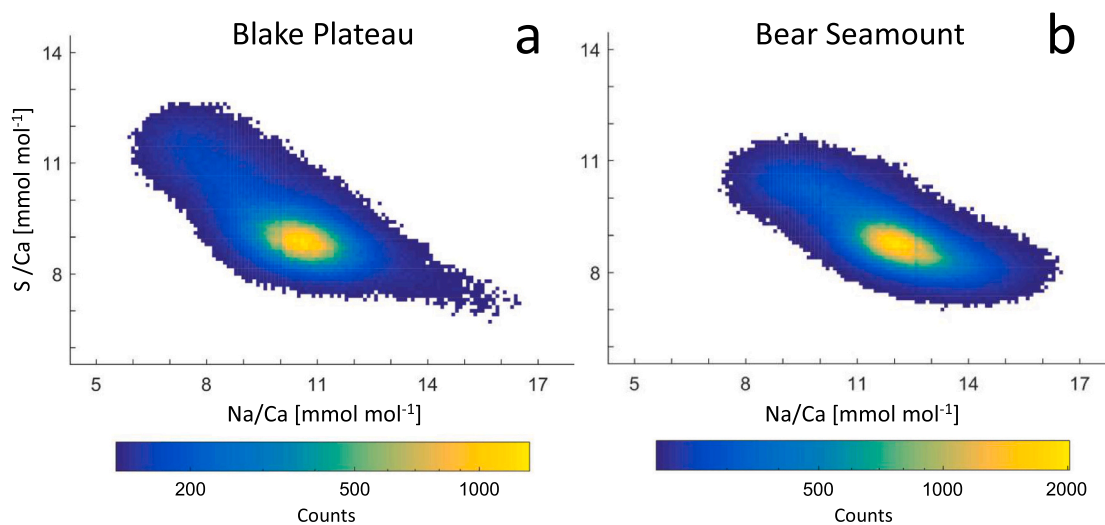
Fig. 4. Sodium to Ca and S/Ca are inversely correlated in bamboo coral samples from the Blake Plateau and the Bear Seamount. The distribution suggests an inverse correlation following a sigmoidal relationship which can be inferred from the frequency distribution. (For interpretation of the references to colour in this figure legend, the reader is referred to the web version of this article.)

crystallographic axis of the measured crystal relative to the polarisation direction of the laser used. Therefore, the relative crystal orientation can be illustrated in an image based on the residual obtained by normalising the intensity of two Raman peaks (Murphy et al., 2021; Nehrke and Nouet, 2011). An image created based on this method in which the Raman peak at 1085 cm^{-1} is normalised to the Raman peak at 285 cm^{-1} shows elongated parallel crystallites in the inner about 4.5 mm of the sample (see Appendix A Fig. A.12). The crystallites are arranged radially to the sample section while a slight wave pattern of the bundles can be observed too. In contrast to this observation, the outer about 1.5 mm of the section shows a less uniform crystallite shape and orientation.

4. Discussion

4.1. Potential environmental drivers of the elemental composition

Recent absolute seawater variation for temperature and salinity on the Blake Plateau (3.9 °C and 0.21 PSU) is higher than that on Bear Seamount (0.9 °C and 0.13 PSU). Similarly, we observe a stronger pronounced banding pattern (Fig. 2) and a higher variation in the Na/Ca composition of the Blake Plateau sample ($\pm$ 3.9 2SD) compared to the Bear Seamount sample ($\pm$ 3.3 2SD). This could indicate a response of skeletal Na/Ca and S/Ca to environmental factors, although a long list of possible factors besides temperature and salinity could equally be responsible. These include ambient nutrient availability, predation, and dynamics of the associated microbiome, oxygen concentration, or pH. Although information towards these additional parameters is not available, chemical patterns distributed along regions of presumed simultaneous growth suggest that these Na/Ca and S/Ca patterns are only to a minor extent directly governed by environmental factors. Therefore, most likely internal drivers i.e., physiological processes seem to be the most important factors creating the observed element distribution.

In the following, we will discuss potential driving mechanisms and describe a model that can explain the observed elemental distribution in context with the distribution of organic matter in the skeleton.

4.2. Insights from the apparent distribution coefficients

The partitioning of Na and S into carbonates was investigated in several previous studies that included biogenic (e.g. Rollion-Bard and Blamart (2015) for Na and van Dijk et al. (2017) for S) and abiogenic calcite (e.g. Ishikawa and Ichikuni (1984) for Na and Kitano et al. (1975) for S). Comparing the K_D^* from different species can give information about potential similarities of the calcification mechanism.

For interstudy comparisons, uniform calculations of the mean K_D^* are needed. For that, the activity and not the concentration should be used. This approach is required since ions with unequal activity coefficients, but the same concentrations behave differently during precipitation. Nevertheless, the activity coefficients in the calcifying fluid of bamboo corals are not known yet due to their unspecified composition. When comparing calcium carbonates precipitated from different precipitation solutions this can result in uncertainties for the interpretation of the underlying calcification mechanism. This is the reason why we use the term "apparent" for the distribution coefficients (a discussion on using an "apparent" distribution coefficient in this context can be found in Langer et al. (2006)). The results of this comparison are nevertheless useful but must be taken with caution when comparing results from experiments and organisms with (potentially) different fluid compositions (see Langer et al. (2018)).

To compare the K_D^* of our *Keratoisis* samples with other calcitic octocorals we used the published Na and S concentrations of two different *Corallium* species from Vielzeuf et al. (2018) as well as Na concentrations of bamboo corals from Rollion-Bard et al. (2017) and calculated the respective Na/Ca and S/Ca K_D^*'s. We must emphasize that — although being small — the gained K_D suggests significant

variations of the spatial element distribution and skeletal composition. This is indicated by the well-defined similar spatial patterns of Na and S beyond their 2SD concentration measurement uncertainty of 9 and 7% respectively. The Na composition of bamboo corals was also investigated by Rollion-Bard et al. (2017). These authors report skeletal Na concentrations measured by secondary ion mass spectrometry (SIMS) and ICP-MS resulting in a K_D^* of 2.8 to 4.1*10^{-4} slightly higher than the mean value we found. Using the published data of *Corallium elatius* from the Tosa Bay (Japan) revealed a K_D^* of Na of about 1.9 to 3.9*10^{-4} and the *C. rubrum* sample "Medes2014" (Spain) showed a K_D^* of about 2.1 to 3.8*10^{-4}. Therefore, the values of the *Keratoisis* samples in this study (1.9 to 3.3*10^{-4}) fall within the range of published *Corallium* specimens. Sulfur shows a similar K_D^* in the samples from Vielzeuf et al. (2018) compared to the bamboo corals of this study. We found a range of 3.2 to 4.5*10^{-3} while the data from Vielzeuf et al. (2018) yield K_D's of 2.9 to 4.8*10^{-3}.

The similarities in Na and S partitioning between the investigated octocoral species indicate a similar calcification mechanism. Nevertheless, a comparison with actual distribution coefficients (K_D) from abiotic precipitation appears to be more useful to make conclusions on the hypothetical calcifying fluid composition and its changes rather than using values from other calcifying organisms where the processes behind the change are more complex. The mean K_D^* for Na in our two NW Atlantic samples (2.5 and 2.8*10^{-4}) fall within the range of values from precipitation experiments for abiotic calcite. Kitano et al. (1975) found K_D's of 0.7–0.9*10^{-4}, Busenberg and Plummer (1985) 13.1*10^{-4} and Okumura and Kitano (1986) 0.6*10^{-4}. It has to be noted that the range of the K_D's is largely extended by the value from Busenberg and Plummer (1985). The chosen literature values are those closest to seawater conditions although only the experimental conditions of Kitano et al. (1975) were matching the concentration of Na in seawater. These values of different studies were selected for comparison since it is generally assumed that the composition of the calcifying fluid is close to seawater (e.g., Cohen et al., 2006; Erez and Braun, 2007; Rollion-Bard et al., 2010). Busenberg and Plummer (1985) explained the range of different reported distribution coefficients in the different studies by varying numbers of defect sites where Na is incorporated, which can for example be driven by precipitation rate. The mean skeletal K_D^* of Na falling in the range of abiotic calcites indicates that the skeletal Na composition is mostly driven by physicochemical parameters of the calcifying fluid that were changed during the precipitation experiments as well. These known drivers of crystal composition can be used to estimate the cause of Na variations in the skeleton. Therefore, bamboo corals have the potential to record environmental conditions that have a direct impact on the calcifying fluid properties in their skeletal Na/Ca ratio. We must admit that a quantitative calibration is beyond the scope of this study.

The mean K_D^*'s for S found in our study are with 3.6 and 3.8*10^{-3} above the range of observed values for synthetic calcite presented by Wynn et al. (2018). These authors reported values of about 0.5 to 10*10^{-4} which is similar to the range of 0.1 to 8*10^{-4} by Busenberg and Plummer (1985). Both studies found a strong positive correlation with the precipitation rate. Further, the rising sulfate concentration of the precipitation solution was reported to increase the S content of precipitated calcite (e.g., Kitano et al. (1975); Kontrec et al., 2004; Okumura et al., 2018). Further, it was observed by Kitano et al. (1975) that a rising Na content of the precipitation solution decreases the S concentration in the formed calcite. This finding indicates that the interpretation of precipitation studies should be treated with caution since none of the above-mentioned publications created seawater-like conditions for Na and S at the same time during precipitation. For bamboo corals, we assume that the S concentration in the calcifying fluid is approximately kept constant. This assumption can be made since only minor S quantities are consumed during the calcification process. This excludes concentration variations in the calcifying fluid as a potential source of S variability in the skeleton. In abiotic precipitation studies, the K_D's of Na

and S are similarly driven by precipitation rate, i.e. both elements show an increasing concentration with precipitation rate. Therefore, their observed inverse correlation in bamboo coral skeletons is not directly caused by the precipitation rate (cf. Fig. 4). Based on these findings it can nevertheless not be excluded that only either Na/Ca or S/Ca in bamboo corals is driven by precipitation rate.

A factor closely related to precipitation rate could also lead to enrichment or depletion of one of both elements respectively resulting in an inverse correlation. This factor could for example be controlled by the increased formation of S-rich organic matter during times of lower calcite precipitation rates. Increasing concentrations of S-rich skeletal organic matter dilute the calcite fraction in the skeleton and with that, the calcium carbonate associated Na leads to an inverse Na—S distribution. An indicator for the contribution of organic S to the total S concentration in bamboo coral calcitic skeletons is the (at least three-fold) elevated K_D^* of S in comparison with abiotically precipitated calcite. From the spatial distribution of S, it can be inferred that the corresponding K_D^*'s are always higher than the highest K_D found in abiotic precipitation experiments. This implies that if the increased K_D^* indicates the presence of organic matter it can be found in the whole skeleton. If in addition, organic matter impacts the elemental distribution this would influence the whole calcitic skeleton and would not be restricted to a few sites.

Despite the limitation given through the unknown activity of Na and S these considerations already indicate that a combination of multiple effects can lead to the observed spatial element distribution.

4.3. Potential internal drivers

Several mechanisms have been tested to explain the distribution of Na in comparison with other metal ions and S in biogenic calcium carbonates. Besides precipitation rate effects, which we already discussed in the previous section, Rayleigh fractionation, pH change in the calcifying fluid, ion-specific pumping, and carrier phase mixing have previously been considered (e.g. Allen et al., 2016; Rollion-Bard and Blamart, 2015; Vielzeuf et al., 2018).

One possible internal influence is Rayleigh fractionation with and without Ca-pumping which was considered by Gagnon et al. (2012) and Rollion-Bard and Blamart (2015). In the calcification models discussed in these publications, Na and S are regarded as conservative elements in the semi-enclosed calcifying fluid, while Ca, as well as carbonate ions, are successively removed from the calcifying fluid by precipitation. The absolute concentration of Na and S in the calcifying fluid does not change due to physiological processes. Rayleigh fractionation as a major control falls short since the Ca removal by precipitation would cause a residual enrichment of both, Na and S, thereby leading to a positive correlation. For an inverse correlation, the distribution coefficient for either Na or S had to be smaller than one, while the other would have to be larger. Based on the skeletal and SW concentrations of Na, S, and Ca both K_D^*'s are significantly smaller than one.

Another model we considered to constrain the Na—S distribution in bamboo corals was the Ca/proton exchange model (see e.g., McConnaughey and Whelan (1997) or Zoccola et al. (2004)). This model was also recently applied by Giri and Swart (2019) to explain the sulfate incorporation into scleractinian coral skeletons. In this model Ca is pumped into the calcifying fluid in exchange for two protons. This raises the pH and accelerates CO_2 flux into the calcifying fluid which in presence of carbonic anhydrases reacts to bicarbonate. As a result, the S/C and the Na/Ca ratio in the calcifying fluid would be lowered causing a positive correlation in the elemental composition of the skeleton. Given that such elemental trends are not seen in our specimens this model also cannot explain the observed patterns.

Ion-specific pumping of Na and S that results in an enrichment of S in the calcifying fluid while depleting Na also seems unlikely. It is known that sulfate inhibits calcite growth in concert with Mg at seawater concentrations (Nielsen et al., 2016). Active depletion of sulfate or Mg in the calcifying fluid would therefore allow the bamboo coral to easier precipitate calcite. Zeebe and Sanyal (2002) described that active Mg depletion is less effective than proton removal from artificial seawater to precipitate calcite. This indicates that proton removal is the most efficient way to increase the saturation state of the calcifying fluid. Further, active sulfate pumping is to the best of our knowledge only described for scleractinian corals and elevated in presence of zooxanthellate symbionts (e.g. Yuyama et al., 2016) which are not present in bamboo corals. In scleractinians, sulfate was found to be transferred into the soft tissue from the culturing medium (Yuyama et al., 2016). Seawater contains high concentrations of sulfate that effectively will not change due to the transfer of the coral because of its large reservoir size. Therefore, the comparably small reservoir of the calcifying fluid does not seem to be a reasonable source of sulfate for the potential sulfate demand of a bamboo coral. Therefore, we assume in the following that ion-specific transport of S from or to the calcifying fluid does not take place. Even if Na is involved in Ca pumping by Na/Ca exchange (Barron et al., 2018; Marshall, 1996) this would not result in the observed inverse correlation. This is because the depletion of Na in favour of Ca would lead to a lower S/Ca ratio. Therefore, this would rather result in a direct correlation than in the observed inverse Na—S pattern.

4.4. A bamboo coral calcification model

After the exclusion of inefficient mechanisms, the cause of the Na—S inverse correlation can involve two separate mechanisms. The first mechanism involves calcite formation from a reservoir with ion exchange and the second one involves the formation of organic matter in the skeletal matrix. To verify this hypothesis, we employ the scleractinian coral calcification model of McCulloch et al. (2017) and include both mechanisms. In line with the published model, we suggest that skeletal calcite formation takes place in a finite reservoir confined by a tissue layer and the skeleton such as proposed earlier (e.g., Barnes, 1970; Clode and Marshall, 2002; Cohen and McConnaughey, 2003). This finite reservoir has an initial composition of seawater (Cohen et al., 2006; Erez and Braun, 2007; Rollion-Bard et al., 2010). Further, we assume that Na and S are only removed by co-precipitation with calcite and are not actively regulated in the calcifying fluid.

To illustrate our calcification model for bamboo corals (Fig. 5), we use a sequential development of the fluid conditions. Nevertheless, under real-life conditions we assume this development to happen simultaneously. Our calcification model starts with seawater input to the calcifying fluid. Subsequently, the Ca concentration and the pH rise in the calcifying fluid through the activity of Ca/proton-pumps (Cohen and McConnaughey, 2003). The rising pH leads to a shift in the carbonate equilibrium allowing for the diffusion of additional carbonate ions into the calcifying fluid. This leads to a higher calcite saturation which favours a faster precipitation rate (Teng et al., 2000; van der Weijden and van der Weijden, 2014). To keep Ca stable at a high concentration it is pumped into the calcifying fluid which compensates for the loss during precipitation. This has two implications for Na. The first is that the Na/Ca ratio in the calcifying fluid is lower than that of seawater. Due to seawater leakage into the calcifying fluid and a small uptake into the calcite, the Na concentration of the calcifying fluid stays at seawater concentration. Consequently, Na/Ca mainly reflects the Ca enrichment in the calcifying fluid. The second implication is the enhanced formation of defect sites during elevated calcification, which leads to a higher rate of Na incorporation (Füger et al., 2019). The increase of precipitation rate influences S incorporation as well. Based on the findings of Wynn et al. (2018) who investigated pH-dependent sulfate incorporation into calcite we could assume that the rate-dependent formation of defect sites also leads to the increased incorporation of S. Since Na and S are inversely correlated, we suggest that defect-site related incorporation plays at most only a minor role during Na and S incorporation. Instead, we favour a different explanation.

In the following, we develop an explanation that is based on a
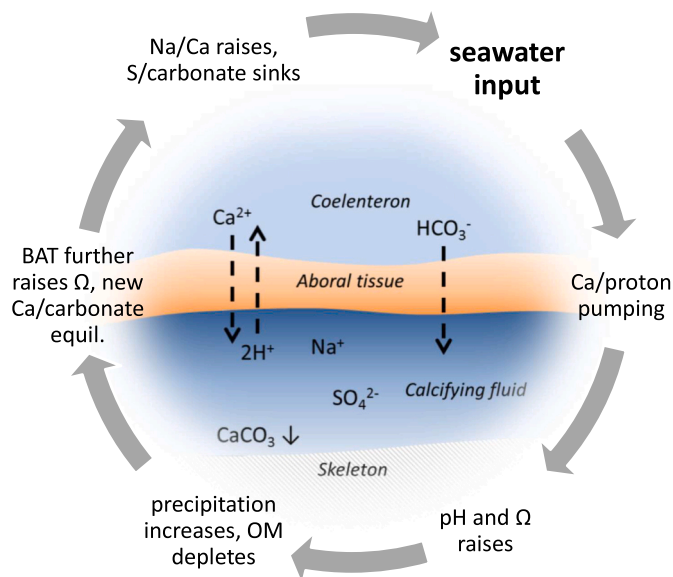
Fig. 5. Proposed calcification model for bamboo corals applied to Na and S. This model adopts an earlier model for scleractinian corals from McCulloch et al. (2017) and extends its implications to the latter two elements and the organic matrix (OM). Bicarbonate active transport is abbreviated BAT and Ω denotes the calcite saturation state. The sequence is intended to illustrate how an inverse distribution occurs. Under real-life conditions, we assume that BAT and Ca/proton pumping happen at the same time.

combination of bicarbonate active transport (BAT) in addition to Ca/proton pumping. It has to be emphasised that BAT plays a central role in our calcification model to explain the inverse Na—S relation. To keep the calcite saturation high and the buffer capacity of the calcifying fluid stable, BAT delivers bicarbonate to the calcifying fluid (Zoccola et al., 2015). The transport of bicarbonate, therefore, supports the Ca/proton pumping in regulating the calcite saturation state of the calcifying fluid. The latter already increases the carbonate ion concentration by shifting the calcifying fluid pH which leads to a decrease in the calcifying fluid S/carbonate ratio. To date, all published $\delta^{11}B$ values of octocorals indicate a smaller pH increase of the calcifying fluid than for scleractinian corals (e.g. McCulloch et al., 2012). For example, Rollion-Bard et al. (2017) report an increase of about 0.4 pH units for the bamboo coral *Isidella* sp. while McCulloch et al. (2012) found a pH increase in different scleractinians between 0.7 and 1.1 units. The average offset of octocoral carbonate to seawater $\delta^{11}B_{borate}$ at the respective sample location from McCulloch et al. (2012), Farmer et al. (2015a, 2015b), Rollion-Bard et al. (2017), and Saenger et al. (2017) gives a positive value of about 0.7‰. This value further indicates a slight pH increase of the calcifying fluid with respect to seawater as assumed in our model. Additionally, BAT can lead to the transport of borate to the calcifying fluid and with that to an apparently low or absent pH upregulation when reconstructed by the $\delta^{11}B_{borate}$-pH proxy (Fietzke and Wall, 2022).

The interplay of BAT and Ca/proton pumping can lead to different Ca/carbonate ratios in the calcifying fluid at the same calcite saturation level. The Ca/carbonate ratio only depends on the respective strength of activity of the two processes. Further, we assume a calcifying fluid state where Ca/proton pumping, and precipitation of calcite are in equilibrium. When BAT is supporting Ca/proton pumping, the saturation and thus, the precipitation rate increases, leading to an increased outflux of Ca and carbonate ions without an increase of Ca influx. This is followed by a new equilibrium with a lower relative amount of Ca but a higher carbonate concentration in the solution. The calcifying fluid will therefore have a lower S/carbonate and higher Na/Ca ratio than without BAT. Hence, only the coupling of Ca/proton pumping in combination with BAT eventually leads to an inverse correlation of Na/Ca and S/

carbonate in the calcifying solution. A variable activity of Ca/proton pumping alone would not result in this inverse correlation.

To link the fluid composition with that of the skeleton we assume that in the calcite lattice Ca and carbonate are being equimolar. In our model the skeletal S/Ca ratio and therefore the skeletal S/carbonate decreases with rising pH and carbonate concentration in the calcifying fluid. This is in line with the results of abiotic calcite precipitation experiments by (Wynn et al., 2018). Therefore, changes in calcifying fluid S/carbonate ratios will result in changes of skeletal S/carbonate and with that S/Ca ratios. Our model predicts at high rates of Ca/proton pumping and low BAT a low skeletal Na/S ratio. In contrast, at low Ca/proton pumping and high BAT a high skeletal Na/S ratio will be established.

The second mechanism for the explanation of the inverse correlation involves the formation of a collagen-like substance in the skeleton and the admixture of calcite and organic material. This mechanism is included in the modified model at the step where the precipitation rate increases (Fig. 5). Most organically bound sulfate is contained in the acidic polysaccharide chondroitin sulfate (e.g., Dauphin, 2006; Perrin et al., 2017). The formation of organic matter-rich growth layers will therefore enrich sulfate in the skeleton. This is in line with our observation that high S-regions correlate with high fluorescence, an indicator for organic matter content. Nevertheless, most S in calcitic octocorals is found to be present as inorganic sulfate (e.g., Nguyen et al., 2014; Balan et al., 2017; Perrin et al., 2017). Nguyen et al. (2014) reported a ratio of one part organic S to 20 parts inorganic S for the calcitic octocoral *Paracorallium japonicum*. Due to this S is not regarded as a robust indicator for organic matter distribution in our samples. Although the mean concentration of organic matter in the calcitic skeleton is supposed to be low, local strong enrichment cannot be excluded.

Based on CRM mapping S seems to be enriched at sites with high concentrations of fluorescent organic matter. Nevertheless, this does not necessarily mean that at sites of low fluorescence there is less organic matter. The following should be considered concerning the fluorescence distribution determined by Raman spectroscopy. It has been demonstrated that some structures from which the presence of organic molecules is well known, like the centres of calcification (also called early mineralization zone) of scleractinian corals do show strong fluorescence when imaged by confocal Raman microscopy (Wall and Nehrke, 2012). However, the fact that certain organic molecules show enhanced fluorescence if irradiated with photons of a certain wavelength does not mean that all types of organic molecules present do. A systematic study that investigates the response of organic molecules present in biogenic minerals to irradiation with photons of different wavelengths is not available. Therefore, one should be careful to relate the strength of a fluorescent signal quantitatively and to deduce the absence of organic molecules based on the absence of fluorescence.

To make inferences on the distribution of fluorescent organic matter in the skeleton we assume in the following, that the fluorescence properties of the organic matter in the skeleton are constant. This organic matter would be diluted, as indicated by less fluorescence, by an increased precipitation rate. In contrast, during times of enhanced organic matter build-up, the calcite portion in the formed skeletal material decreases. Based on the spatial resolution of used analytical techniques the organic matter-S relation can nevertheless be a coincidence. The latter can also be explained by an increase of inorganic S in the interstitial calcite by low BAT activity. The presence of at least two possibilities indicates that mixing calcitic and organic phases is unlikely to be the only driver of the observed inverse correlation of Na and S. Since the K_D^{*}'s of S point towards a general increase of the S concentration by organic matter the theory of solely interstitial calcite driving this process is unlikely. It rather supports a combined influence of organic matter dilution and BAT on the skeletal S distribution and concentration.

It was found that besides S organic matter influences the trace metal concentration in biogenic carbonates as well. Contrary to the findings

for trace metals such as Sr and Ba in scleractinians (e.g. Meibom et al., 2006, 2008; Finch and Allison, 2008), Na is depleted in regions of higher S concentrations and potential organic matter enrichment. A similar finding was made for intraskeletal foraminiferal organic matter. Their primary organic sheet coincides with a high Na/Ca (Bonnin et al., 2019). Therefore, the depletion of Na in the potentially organic-rich matter would have to be a specific property of organic matter in bamboo corals. This cannot be excluded but seems to be unlikely. This comparison further supports the assertion that at least the Na distribution in bamboo corals is not solely driven by organic matter.

Given the above line of reasoning, we suggest that both mechanisms, the first including dilution and kinetic effects and the second based on organic matter build-up, are deemed to influence the Na and S composition of bamboo coral skeletons. The first one likely dominates during times of high growth rates while the latter one requires more energy and takes place during times of high energy supply. Therefore, the energy-demanding process of gametogenesis for spawning must be considered as a potential influence on Na and S distribution. Indeed, this hypothesis is supported by scleractinian corals which build up tissue preferentially under the highest nutrient conditions, calcify and reproduce under moderate conditions and focus on calcification under low nutrient conditions (e.g. Leuzinger et al., 2012). Further, already Tracey et al. (2007) suggest that reproduction may influence the element composition in bamboo corals. Since Mercier and Hamel (2011) found an annual cycle of reproduction in a Canadian bamboo coral (*Keratoisis ornata*) an annual cycle in Na and S concentration would be in line with our hypothesis.

A test of our model can be carried out by using already published compositional data, e.g. from Rollion-Bard et al. (2017). These authors found a positive correlation of Na/Ca, Li/Ca, and Mg/Ca in bamboo coral internodes. In the calcifying fluid of our model Na, Mg, and Li are thought to behave passively while only pH, Ca, and bicarbonate are actively regulated. The low distribution coefficient of below one for all these elements in calcite would accordingly result in a positive correlation as is observed by Rollion-Bard et al. (2017).

5. Conclusion

This study investigated the elemental distribution of Na/Ca and S/Ca in the internodes of two Atlantic bamboo corals at the microscale to evaluate the proxy potential of these elements and the drivers of their incorporation. Further, the existing calcifications models were tested to correctly predict the Na and S composition.

Sodium was found to be incorporated into the calcitic skeleton with partitioning coefficients that fall in the range of abiotically precipitated calcite while S was found to be enriched. Based on the K_D^*'s of Na it is therefore assumed that Na has the potential for being used as an environmental proxy in bamboo corals. The difference of relative variability of salinity at the sampling sites is tentatively reflected in the skeletal variability of Na/Ca from samples of the respective sites. Nevertheless, a coincidence cannot be excluded and investigations with a greater number of samples would have to confirm this hypothesis. Strikingly, chemical variations along growth rings rule out an exclusive environmental impact on these small-scale patterns. Given our mapping and quantitative model results we propose that skeletal Na/Ca and S/Ca are dominated by physiological processes within bamboo corals rather than by ambient salinity or temperature.

We found Rayleigh fractionation, ion-specific pumping of Na and S, and Ca/proton exchange not to be responsible for the observed Na—S inverse correlation. We rather suggest a calcification model that is based on that of McCulloch et al. (2017). This modified model is capable of successfully describing the observed inverse Na—S correlation. Intraskeletal organic matter had to be incorporated into this model to explain all the observed compositional properties. Nevertheless, chemical mapping using a higher spatial resolution and investigations of the spatial distribution of the different S species are required in future studies to gain a better understanding of the relation of S and organic matter in bamboo corals.

The here proposed modified calcification model can be used in future studies on the potential of bamboo corals as an environmental archive on additional elemental environmental proxies. It allows to predict element behaviour and can help to separate environmental from physiological drivers of the calcitic skeletal composition.

Declaration of Competing Interest

The authors declare that they have no known competing financial interests or personal relationships that could have appeared to influence the work reported in this paper.

Appendix A. Supplementary data

Supplementary data to this article can be found online at https://doi. org/10.1016/j.chemgeo.2022.120795.

References

Allen, K.A., Hönisch, B., Eggins, S.M., Haynes, L.L., Rosenthal, Y., Yu, J.M., 2016. Trace element proxies for surface ocean conditions: a synthesis of culture calibrations with planktic foraminifera. Geochim. Cosmochim. Acta 193, 197–221. https://doi.org/ 10.1016/j.gca.2016.08.015.

Andrews, A.H., Stone, R.P., Lundstrom, C.C., DeVogelaere, A.P., 2009. Growth rate and age determination of bamboo corals from the northeastern Pacific Ocean using refined ^{210}Pb dating. Mar. Ecol. Prog. Ser. 397, 173–185. https://doi.org/10.3354/ meps08193.

Balan, E., Aufort, J., Pouillé, S., Dabos, M., Blanchard, M., Lazzeri, M., Rollion-Bard, C., Blamart, D., 2017. Infrared spectroscopic study of sulfate-bearing calcite from deep-sea bamboo coral. Eur. J. Mineral. 29, 397–408. https://doi.org/10.1127/ejm/ 2017/0029-2611.

Ballesta-Artero, I., Zhao, L., Milano, S., Mertz-Kraus, R., Schone, B.R., van der Meer, J., Witbaard, R., 2018. Environmental and biological factors influencing trace elemental and microstructural properties of *Arctica islandica* shells. Sci. Total Environ. 645, 913–923. https://doi.org/10.1016/j.scitotenv.2018.07.116.

Barnes, D.J., 1970. Coral skeletons: an explanation of their growth and structure. Science 170, 1305–1308. https://doi.org/10.1126/science.170.3964.1305.

Barron, M.E., Thies, A.B., Espinoza, J.A., Barott, K.L., Hamdoun, A., Tresguerres, M., 2018. A vesicular Na$^+$/Ca^{2+} exchanger in coral calcifying cells. PLoS One 13, e0205367. https://doi.org/10.1371/journal.pone.0205367.

Bonnin, E.A., Zhu, Z., Fehrenbacher, J.S., Russell, A.D., Hönisch, B., Spero, H.J., Gagnon, A.C., 2019. Submicron sodium banding in cultured planktic foraminifera shells. Geochim. Cosmochim. Acta 253, 127–141. https://doi.org/10.1016/j. gca.2019.03.024.

Bostock, H.C., Tracey, D.M., Currie, K.I., Dunbar, G.B., Handler, M.R., Fletcher, S.E.M., Smith, A.M., Williams, M.J.M., 2015. The carbonate mineralogy and distribution of habitat-forming deep-sea corals in the Southwest Pacific region. Deep-Sea Res. Part -Oceanogr. Res. Pap. 100, 88–104. https://doi.org/10.1016/j.dsr.2015.02.008.

Busenberg, E., Plummer, L.N., 1985. Kinetic and thermodynamic factors controlling the distribution of SO_3^{2-} and Na$^+$ in calcites and selected aragonites. Geochim. Cosmochim. Acta 49, 713–725. https://doi.org/10.1016/0016-7037(85)90166-8.

Clode, P.L., Marshall, A.T., 2002. Low temperature FESEM of the calcifying interface of a scleractinian coral. Tissue Cell 34, 187–198. https://doi.org/10.1016/S0040-8166 (02)00031-9.

Cohen, A.L., McConnaughey, T.A., 2003. Geochemical perspectives on coral mineralization. Biomineralization 54, 151–187. https://doi.org/10.2113/0540151.

Cohen, A.L., Gaetani, G.A., Lundalv, T., Corliss, B.H., George, R.Y., 2006. Compositional variability in a cold-water scleractinian, *Lophelia pertusa*: new insights into "vital effects.". Geochem. Geophys. Geosyst. 7 https://doi.org/10.1029/2006gc001354.

Cusack, M., Dauphin, Y., Cuif, J.P., Salome, M., Freer, A., Yin, H., 2008. Micro-XANES mapping of sulphur and its association with magnesium and phosphorus in the shell of the brachiopod, *Terebratulina retusa*. Chem. Geol. 253, 172–179. https://doi.org/10.1016/j.chemgeo.2008.05.007.

Dauphin, Y., 2006. Mineralizing matrices in the skeletal axes of two Corallium species (Alcyonacea). Comp. Biochem. Physiol. A. Mol. Integr. Physiol. 145, 54–64. https://doi.org/10.1016/j.cbpa.2006.04.029.

Eggins, S.M., Kinsley, L.P.J., Shelley, J.M.G., 1998. Deposition and element fractionation processes during atmospheric pressure laser sampling for analysis by ICP-MS. Appl. Surf. Sci. 127–129, 278–286. https://doi.org/10.1016/S0169-4332(97)00643-0.

Erez, J., Braun, A., 2007. Calcification in hermatypic corals is based on direct seawater supply to the biomineralization site. Geochim. Cosmochim. Acta 71, A260.

Farmer, J.R., Hönisch, B., Robinson, L.F., Hill, T.M., 2015a. Effects of seawater-pH and biomineralization on the boron isotopic composition of deep-sea bamboo corals. Geochim. Cosmochim. Acta 155, 86–106. https://doi.org/10.1016/j.gca.2015.01.018.

Farmer, J.R., Robinson, L.F., Hönisch, B., 2015b. Growth rate determinations from radiocarbon in bamboo corals (genus Keratoisis). Deep-Sea Res. Part -Oceanogr. Res. Pap. 105, 26–40. https://doi.org/10.1016/j.dsr.2015.08.004.

Fichtner, V., Strauss, H., Mavromatis, V., Dietzel, M., Huthwelker, T., Borca, C.N., Guagliardo, P., Kilburn, M.R., Gottlicher, J., Pederson, C.L., Griesshaber, E., Schmahl, W.W., Immenhauser, A., 2018. Incorporation and subsequent diagenetic alteration of sulfur in *Arctica islandica*. Chem. Geol. 482, 72–90. https://doi.org/10.1016/j.chemgeo.2018.01.035.

Fietzke, J., Frische, M., 2016. Experimental evaluation of elemental behavior during LA-ICP-MS: influences of plasma conditions and limits of plasma robustness. J. Anal. At. Spectrom. 31 (1), 234–244. https://doi.org/10.1039/C5JA00253B.

Fietzke, J., Wall, M., 2022. Distinct fine-scale variations in calcification control revealed by high-resolution boron laser images in cold-water coral *L. pertusa*. Sci. Adv. 8 (11) https://doi.org/10.1126/sciadv.abj4172. In press.

Finch, A.A., Allison, N., 2008. Mg structural state in coral aragonite and implications for the paleoenvironmental proxy. Geophys. Res. Lett. 35 https://doi.org/10.1029/2008GL033543.

Flöter, S., Fietzke, J., Gutjahr, M., Farmer, J., Hönisch, B., Nehrke, G., Eisenhauer, A., 2019. The influence of skeletal micro-structures on potential proxy records in a bamboo coral. Geochim. Cosmochim. Acta 248, 43–60. https://doi.org/10.1016/j.gca.2018.12.027.

Füger, A., Konrad, F., Leis, A., Dietzel, M., Mavromatis, V., 2019. Effect of growth rate and pH on lithium incorporation in calcite. Geochim. Cosmochim. Acta 248, 14–24. https://doi.org/10.1016/j.gca.2018.12.040.

Gagnon, A.C., Adkins, J.F., Erez, J., 2012. Seawater transport during coral biomineralization. Earth Planet. Sci. Lett. 329–330, 150–161. https://doi.org/10.1016/j.epsl.2012.03.005.

Giri, S.J., Swart, P.K., 2019. The influence of seawater chemistry on carbonate-associated sulfate derived from coral skeletons. Palaeogeogr. Palaeoclimatol. Palaeoecol. 521, 72–81. https://doi.org/10.1016/j.palaeo.2019.02.011.

Giri, S.J., Swart, P.K., Pourmand, A., 2019. The influence of seawater calcium ions on coral calcification mechanisms: Constraints from boron and carbon isotopes and B/ca ratios in *Pocillopora damicornis*. Earth Planet. Sci. Lett. 519, 130–140. https://doi.org/10.1016/j.epsl.2019.05.008.

Gordon, C.M., Carr, R.A., Larson, R.E., 1970. The Influence of Environmental Factors on the Sodium and Manganese Content of Barnacle Shells. Limnol. Oceanogr. 15, 461–466. https://doi.org/10.4319/lo.1970.15.3.0461.

Hauzer, H., Evans, D., Muller, W., Rosenthal, Y., Erez, J., 2018. Calibration of Na partitioning in the calcitic foraminifer *Operculina ammonoides* under variable Ca concentration: toward reconstructing past seawater composition. Earth Planet. Sci. Lett. 497, 80–91. https://doi.org/10.1016/j.epsl.2018.06.004.

Hill, T.M., Spero, H.J., Guilderson, T., LaVigne, M., Clague, D., Macalello, S., Jang, N., 2011. Temperature and vital effect controls on bamboo coral (Isididae) isotope geochemistry: a test of the "lines method.". Geochem. Geophys. Geosyst. 12 https://doi.org/10.1029/2010gc003443.

Hill, T.M., LaVigne, M., Spero, H.J., Guilderson, T., Gaylord, B., Clague, D., 2012. Variations in seawater Sr/Ca recorded in deep-sea bamboo corals. Paleoceanography 27. https://doi.org/10.1029/2011PA002260.

Iglikowska, A., Ronowicz, M., Humphreys-Williams, E., Kuklinski, P., 2018. Trace element accumulation in the shell of the Arctic cirriped *Balanus balanus*. Hydrobiologia 818, 43–56. https://doi.org/10.1007/s10750-018-3564-5.

Ishikawa, M., Ichikuni, M., 1984. Uptake of sodium and potassium by calcite. Chem. Geol. 42, 137–146. https://doi.org/10.1016/0009-2541(84)90010-X.

Kanaya, K., Okayama, S., 1972. Penetration and energy-loss theory of electrons in solid targets. J. Phys. D. Appl. Phys. 5, 43–58. https://doi.org/10.1088/0022-3727/5/1/308.

Kitano, Y., Okumura, M., Idogaki, M., 1975. Incorporation of sodium, chloride and sulfate with calcium carbonate. Geochem. J. 9, 75–84. https://doi.org/10.2343/geochemj.9.75.

Kontrec, J., Kralj, D., Brecevic, L., Falini, G., Fermani, S., Noethig-Laslo, V., Mirosavljevic, K., 2004. Incorporation of inorganic anions in calcite. Eur. J. Inorg. Chem. 2004, 4579–4585. https://doi.org/10.1002/ejic.200400268.

Langer, G., Gussone, N., Nehrke, G., Riebesell, U., Eisenhauer, A., Kuhnert, H., Rost, B., Trimborn, S., Thoms, S., 2006. Coccolith strontium to calcium ratios in *Emiliania huxleyi*: the dependence on seawater strontium and calcium concentrations. Limnol. Oceanogr. 51, 310–320. https://doi.org/10.4319/lo.2006.51.1.0310.

Langer, G., Sadekov, A., Nehrke, G., Baggini, C., Rodolfo-Metalpa, R., Hall-Spencer, J.M., Cuoco, E., Bijma, J., Elderfield, H., 2018. Relationship between mineralogy and minor element partitioning in limpets from an Ischia CO2 vent site provides new insights into their biomineralization pathway. Geochim. Cosmochim. Acta. https://doi.org/10.1016/j.gca.2018.02.044.

Le Roy, N., Ganot, P., Aranda, M., Allemand, D., Tambutté, S., 2021. The skeletome of the red coral *Corallium rubrum* indicates an independent evolution of biomineralization process in octocorals. BMC Ecol. Evol. 21, 1. https://doi.org/10.1186/s12862-020-01734-0.

Lécuyer, C., 2016. Seawater residence times of some elements of geochemical interest and the salinity of the oceans. Bull. Soc. Geol. Fr. 187, 245–259. https://doi.org/10.2113/gssgfbull.187.6.245.

Lee, T.N., Waddell, E., 1983. On Gulf-stream variability and meanders over the Blake Plateau at 30-degrees-N. J. Geophys. Res. 88 (Nc8), 4617–4631. https://doi.org/10.1029/JC088iC08p04617.

Leuzinger, S., Willis, B.L., Anthony, K.R.N., 2012. Energy allocation in a reef coral under varying resource availability. Mar. Biol. 159, 177–186. https://doi.org/10.1007/s00227-011-1797-1.

Marshall, A.T., 1996. Calcification in hermatypic and ahermatypic corals. Science 271, 637–639. https://doi.org/10.1126/science.271.5249.637.

McConnaughey, T.A., Whelan, J.F., 1997. Calcification generates protons for nutrient and bicarbonate uptake. Earth-Sci. Rev. 42, 95–117. https://doi.org/10.1016/S0012-8252(96)00036-0.

McCulloch, M.T., D'Olivo, J.P., Falter, J., Holcomb, M., Trotter, J.A., 2017. Coral calcification in a changing World and the interactive dynamics of pH and DIC upregulation. Nat. Commun. 8, 15686. https://doi.org/10.1038/ncomms15686.

Meibom, A., Yurimoto, H., Cuif, J.P., Domart-Coulon, I., Houlbreque, F., Constantz, B., Dauphin, Y., Tambutté, E., Tambutté, S., Allemand, D., Wooden, J., Dunbar, R., 2006. Vital effects in coral skeletal composition display strict three-dimensional control. Geophys. Res. Lett. 33 https://doi.org/10.1029/2006GL025968.

McCulloch, M., Trotter, J., Montagna, P., Falter, J., Dunbar, R., Freiwald, A., Forsterra, N., Lopez Correa, M., Maier, C., Rüggeberg, A., Taviani, M., 2012. Resilience of cold-water scleractinian corals to ocean acidification: boron isotopic systematics of pH and saturation state up-regulation. Geochim. Cosmochim. Ac. 87, 21–34. https://doi.org/10.1016/j.gca.2012.03.027.

Meibom, A., Cuif, J.P., Houlbreque, F., Mostefaoui, S., Dauphin, Y., Meibom, K.L., Dunbar, R., 2008. Compositional variations at ultra-structure length scales in coral skeleton. Geochim. Cosmochim. Acta 72, 1555–1569. https://doi.org/10.1016/j.gca.2008.01.009.

Mercier, A., Hamel, J.F., 2011. Contrasting reproductive strategies in three deep-sea octocorals from eastern Canada: *Primnoa resedaeformis*, *Keratoisis ornata*, and *Anthomastus grandiflorus*. Coral Reefs 30, 337–350. https://doi.org/10.1007/s00338-011-0724-8.

Mezger, E.M., de Nooijer, L.J., Boer, W., Brummer, G.J.A., Reichart, G.J., 2016. Salinity controls on Na incorporation in Red Sea planktonic foraminifera. Paleoceanography 31, 1562–1582. https://doi.org/10.1002/2016pa003052.

Millero, F.J., Feistel, R., Wright, D.G., McDougall, T.J., 2008. The composition of standard seawater and the definition of the reference-composition salinity scale. Deep-Sea Res. Part -Oceanogr. Res. Pap. 55, 50–72. https://doi.org/10.1016/j.dsr.2007.10.001.

Mitsuguchi, T., Kawakami, T., 2012. Potassium and other minor elements in *Porites* corals: implications for skeletal geochemistry and paleoenvironmental reconstruction. Coral Reefs 31, 671–681. https://doi.org/10.1007/s00338-012-0902-3.

Mitsuguchi, T., Uchida, T., Matsumoto, E., 2010. Na/Ca variability in coral skeletons. Geochem. J. 44, 261–273. https://doi.org/10.2343/geochemj.1.0067.

Murphy, A.E., Jakubek, R.S., Steele, A., Fries, M.D., Glamoclija, M., 2021. Raman spectroscopy provides insight into carbonate rock fabric based on calcite and dolomite crystal orientation. J. Raman Spectrosc. 1–12 https://doi.org/10.1002/jrs.6097.

Nehrke, G., Nouet, J., 2011. Confocal Raman microscope mapping as a tool to describe different mineral and organic phases at high spatial resolution within marine biogenic carbonates: case study on *Nerita undata* (Gastropoda, Neritopsina). Biogeosciences 8, 3761–3769. https://doi.org/10.5194/bg-8-3761-2011.

Nguyen, L.T., Rahman, M.A., Maki, T., Tamenori, Y., Yoshimura, T., Suzuki, A., Iwasaki, N., Hasegawa, H., 2014. Distribution of trace element in Japanese red coral *Paracorallium japonicum* by mu-XRF and sulfur speciation by XANES: Linkage between trace element distribution and growth ring formation. Geochim. Cosmochim. Acta 127, 1–9. https://doi.org/10.1016/j.gca.2013.11.023.

Nielsen, M.R., et al., 2016. Inhibition of calcite growth: combined effects of Mg^{2+} and SO_4^{2-}. Cryst. Growth Des. 16 (11), 6199–6207. https://doi.org/10.1021/acs.cgd.6b00536.

Okumura, M., Kitano, Y., 1986. Coprecipitation of alkali-metal ions with calcium-carbonate. Geochim. Cosmochim. Acta 50, 49–58. https://doi.org/10.1016/0016-7037(86)90047-5.

Okumura, T., Kim, H.J., Kim, J.W., Kogure, T., 2018. Sulfate-containing calcite: crystallographic characterization of natural and synthetic materials. Eur. J. Mineral. 30, 929–937. https://doi.org/10.1127/ejm/2018/0030-2772.

Perrin, J., Rivard, C., Vielzeuf, D., Laporte, D., Fonquernie, C., Ricolleau, A., Cotte, M., Floquet, N., 2017. The coordination of sulfur in synthetic and biogenic Mg calcites: the red coral case. Geochim. Cosmochim. Acta 197, 226–244. https://doi.org/10.1016/j.gca.2016.10.017.

Pingitore, N.E., Meitzner, G., Love, K.M., 1995. Identification of sulfate in natural carbonates by X-ray-absorption spectroscopy. Geochim. Cosmochim. Acta 59, 2477–2483. https://doi.org/10.1016/0016-7037(95)00142-5.

Roberts, J.M., Murray, F., Anagnostou, E., Hennige, S., Gori, A., Henry, L.-A., Fox, A., Kamenos, N., Foster, G.L., 2016. Cold-water corals in an era of rapid global change: Are these the deep ocean's most vulnerable ecosystems? In: Goffredo, S., Dubinsky, Z. (Eds.), The Cnidaria, Past, Present and Future: The World of Medusa and her Sisters. Springer International Publishing, Cham, pp. 593–606. https://doi.org/10.1007/978-3-319-31305-4_36.

Robinson, L.F., Adkins, J.F., Frank, N., Gagnon, A.C., Prouty, N.G., Roark, E.B., van de Flierdt, T., 2014. The geochemistry of deep-sea coral skeletons: a review of vital effects and applications for palaeoceanography. Deep-Sea Res. Part Ii-Top. Stud. Oceanogr. 99, 184–198. https://doi.org/10.1016/j.dsr2.2013.06.005.

Rollion-Bard, C., Blamart, D., 2015. Possible controls on Li, Na, and Mg incorporation into aragonite coral skeletons. Chem. Geol. 396, 98–111. https://doi.org/10.1016/j.chemgeo.2014.12.011.

Rollion-Bard, C., Blamart, D., Cuif, J.P., Dauphin, Y., 2010. In situ measurements of oxygen isotopic composition in deep-sea coral, *Lophelia pertusa*: Re-examination of the current geochemical models of biomineralization. Geochim. Cosmochim. Acta 74, 1338–1349. https://doi.org/10.1016/j.gca.2009.11.011.

Rollion-Bard, C., Cuif, J.-P., Blamart, D., 2017. Optical observations and geochemical data in deep-sea hexa- and octo-coralla specimens. Minerals 7, 154. https://doi.org/10.3390/min7090154.

Rollion-Bard, C., Milner Garcia, S., Burckel, P., Angiolini, L., Jurikova, H., Tomašových, A., Henkel, D., 2019. Assessing the biomineralization processes in the shell layers of modern brachiopods from oxygen isotopic composition and elemental ratios: implications for their use as paleoenvironmental proxies. Chem. Geol. 524, 49–66. https://doi.org/10.1016/j.chemgeo.2019.05.031.

Saenger, C., Gabitov, R.I., Farmer, J., Watkins, J.M., Stone, R., 2017. Linear correlations in bamboo coral $\delta^{13}C$ and $\delta^{18}O$ sampled by SIMS and micromill: evaluating paleoceanographic potential and biomineralization mechanisms using $\delta^{11}B$ and Δ_{47} composition. Chem. Geol. 454, 1–14. https://doi.org/10.1016/j.chemgeo.2017.02.014.

Teng, H.H., Dove, P.M., De Yoreo, J.J., 2000. Kinetics of calcite growth: surface processes and relationships to macroscopic rate laws. Geochim. Cosmochim. Acta 64, 2255–2266. https://doi.org/10.1016/S0016-7037(00)00341-0.

Thresher, R.E., Fallon, S.J., Townsend, A.T., 2016. A "core-top" screen for trace element proxies of environmental conditions and growth rates in the calcite skeletons of bamboo corals (Isididae). Geochim. Cosmochim. Acta 193, 75–99. https://doi.org/10.1016/j.gca.2016.07.033.

Tracey, D.M., Neil, H., Marriott, P., Andrews, A.H., Cailliet, G.M., Sánchez, J.A., 2007. Age and growth of two genera of deep-sea bamboo corals (family Isididae) in New Zealand waters. Bull. Mar. Sci. 81, 393–408.

Urey, H.C., Lowenstam, H.A., Epstein, S., Mckinney, C.R., 1951. Measurement of paleotemperatures and temperatures of the Upper Cretaceous of England, Denmark, and the Southeastern United-States. Geol. Soc. Am. Bull. 62, 399–416. https://doi.org/10.1130/0016-7606(1951)62[399:MOPATO]2.0.CO;2.

van der Weijden, C.H., van der Weijden, R.D., 2014. Calcite growth: rate dependence on saturation, on ratios of dissolved calcium and (bi)carbonate and on their complexes. J. Cryst. Growth 394, 137–144. https://doi.org/10.1016/j.jcrysgro.2014.02.042.

van Dijk, I., de Nooijer, L.J., Boer, W., Reichart, G.J., 2017. Sulfur in foraminiferal calcite as a potential proxy for seawater carbonate ion concentration. Earth Planet. Sci. Lett. 470, 64–72. https://doi.org/10.1016/j.epsl.2017.04.031.

van Dijk, I., Mouret, A., Cotte, M., Le Houedec, S., Oron, S., Reichart, G.-J., Reyes-Herrera, J., Filipsson, H.L., Barras, C., 2019. Chemical heterogeneity of Mg, Mn, Na, S, and Sr in benthic foraminiferal calcite. Front. Earth Sci. 7 https://doi.org/10.3389/feart.2019.00281.

Vielzeuf, D., Garrabou, J., Gagnon, A., Ricolleau, A., Adkins, J., Gunther, D., Hametner, K., Devidal, J.L., Reusser, E., Perrin, J., Floquet, N., 2013. Distribution of sulphur and magnesium in the red coral. Chem. Geol. 355, 13–27. https://doi.org/10.1016/j.chemgeo.2013.07.008.

Vielzeuf, D., Gagnon, A.C., Ricolleau, A., Devidal, J.L., Balme-Heuze, C., Yahiaoui, N., Fonquernie, C., Perrin, J., Garrabou, J., Montel, J.M., Floquet, N., 2018. Growth kinetics and distribution of trace elements in precious corals. Front. Earth Sci. 6 https://doi.org/10.3389/feart.2018.00167.

Wall, M., Nehrke, G., 2012. Reconstructing skeletal fiber arrangement and growth mode in the coral *Porites lutea* (Cnidaria, Scleractinia): a confocal Raman microscopy study. Biogeosciences 9, 4885–4895. https://doi.org/10.5194/bg-9-4885-2012.

Wit, J.C., de Nooijer, L.J., Wolthers, M., Reichart, G.J., 2013. A novel salinity proxy based on Na incorporation into foraminiferal calcite. Biogeosciences 10, 6375–6387. https://doi.org/10.5194/bg-10-6375-2013.

Wynn, P.M., Fairchild, I.J., Borsato, A., Spotl, C., Hartland, A., Baker, A., Frisia, S., Baldini, J.U.L., 2018. Sulphate partitioning into calcite: experimental verification of pH control and application to seasonality in speleothems. Geochim. Cosmochim. Acta 226, 69–83. https://doi.org/10.1016/j.gca.2018.01.020.

Yuyama, I., Higuchi, T., Takei, Y., 2016. Sulfur utilization of corals is enhanced by endosymbiotic algae. Biol. Open 5 (9), 1299–1304. https://doi.org/10.1242/bio.020164.

Zeebe, R.E., Sanyal, A., 2002. Comparison of two potential strategies of planktonic foraminifera for house building: Mg^{2+} or H^+ removal? Geochim. Cosmochim. Acta 66 (7), 1159–1169. https://doi.org/10.1016/S0016-7037(01)00852-3.

Zhao, L., Schöne, B.R., Mertz-Kraus, R., Yang, F., 2017. Insights from sodium into the impacts of elevated pCO₂ and temperature on bivalve shell formation. J. Exp. Mar. Biol. Ecol. 486, 148–154. https://doi.org/10.1016/j.jembe.2016.10.009.

Zoccola, D., Tambutté, E., Kulhanek, E., Puverel, S., Scimeca, J.-C., Allemand, D., Tambutté, S., 2004. Molecular cloning and localization of a PMCA P-type calcium ATPase from the coral *Stylophora pistillata*. Biochim. Biophys. Acta Biomembr. 1663, 117–126. https://doi.org/10.1016/j.bbamem.2004.02.010.

Zoccola, D., Ganot, P., Bertucci, A., Caminiti-Segonds, N., Techer, N., Voolstra, C.R., Aranda, M., Tambutte, E., Allemand, D., Casey, J.R., Tambutte, S., 2015. Bicarbonate transporters in corals point towards a key step in the evolution of cnidarian calcification. Sci. Rep. 5, 9983. https://doi.org/10.1038/srep09983.